



**HAL**  
open science

# About the tensile mechanical behaviour of carbon fibers fabrics reinforced thermoplastic composites under very high temperature conditions

Y. Carpier, Benoît Vieille, A. Coppalle, Fabrice Barbe

## ► To cite this version:

Y. Carpier, Benoît Vieille, A. Coppalle, Fabrice Barbe. About the tensile mechanical behaviour of carbon fibers fabrics reinforced thermoplastic composites under very high temperature conditions. *Composites Part B: Engineering*, 2020, 181, pp.107586. 10.1016/j.compositesb.2019.107586. hal-02357075

**HAL Id: hal-02357075**

**<https://hal.science/hal-02357075>**

Submitted on 21 Jul 2022

**HAL** is a multi-disciplinary open access archive for the deposit and dissemination of scientific research documents, whether they are published or not. The documents may come from teaching and research institutions in France or abroad, or from public or private research centers.

L'archive ouverte pluridisciplinaire **HAL**, est destinée au dépôt et à la diffusion de documents scientifiques de niveau recherche, publiés ou non, émanant des établissements d'enseignement et de recherche français ou étrangers, des laboratoires publics ou privés.



Distributed under a Creative Commons Attribution - NonCommercial 4.0 International License

1 **About the tensile mechanical behaviour of carbon fibers fabrics reinforced thermoplastic composites**  
2 **under very high temperature conditions**

3 Y. Carpiert<sup>1</sup>, B. Vieille<sup>1</sup>, A. Coppalle<sup>2</sup>, F. Barbe<sup>1</sup>

4 <sup>1</sup>Normandie Univ, UNIROUEN, INSA Rouen, CNRS, Groupe de Physique des Matériaux, 76000 Rouen,  
5 France

6 <sup>2</sup>Normandie Univ, UNIROUEN, INSA Rouen, CNRS, CORIA, 76000 Rouen, France

7 \*Correspondence to: benoit.vieille@insa-rouen.fr

8

9 **Abstract**

10 The present work focuses on the thermomechanical behaviour of thermoplastic-based composite materials  
11 subjected to the combined action of a mechanical loading in tension and homogeneous temperature  
12 conditions. The investigations on the relationship between local temperature resulting from the local  
13 atmosphere and the mass losses are essential in understanding the influence of fire on the thermo-  
14 mechanical behaviours of polymers and polymer matrix composites. Regardless the testing atmosphere, the  
15 decomposition onset temperature is about 500°C. From isothermal tensile tests conducted at temperatures  
16 ranging from ambient to 520°C, it appears that the retention of the axial stiffness of quasi-isotropic carbon  
17 fibers reinforced polyphenylene sulfide (PPS) laminates is relatively high (about 70% of its initial value)  
18 beyond the decomposition temperature. At the same time, the ultimate strength dramatically decreases  
19 (about 25% of its initial value). The obtained results also show that melting is instrumental to rule the  
20 tensile behavior of quasi-isotropic C/PPS laminates. Conversely, matrix melting significantly influences the  
21 damage mechanisms within the laminate. Finally, for testing temperatures close to the onset decomposition  
22 temperature, porosities appear and grow within the laminates, ultimately contributing to the degradation of  
23 the mechanical properties.

24

25 **Keywords:** thermoplastic; thermal decomposition; high temperature; mechanical behavior, damage

26

## 27 **1. Introduction**

28 The study of fire resistance aims at understanding and characterizing how and for how long the composite  
29 material can bear a mechanical loading when it is subjected to heat fluxes resulting in temperature  
30 differences through-the-thickness. Most Polymer Matrix Composite (PMC) materials usually cannot bear  
31 significant mechanical loading at temperature higher than 200-250°C. High-performance thermoplastic-  
32 based (TP) composites (e.g. PEEK, PPS, PEI...) are promising materials for structural applications in  
33 aeronautics as they are resistant to impact. They have a good damage tolerance as well as they have a very  
34 good retention of their mechanical properties under fire conditions. Among the most common PMCs used  
35 in load-bearing aircraft structures, Carbon/epoxy (thermosetting) composites are flammable and readily  
36 decompose when exposed to heat and fire. The literature dealing with the fire behavior of composite  
37 materials focuses mainly on thermosetting-based composites [1] and rarely on thermoplastic-based  
38 composites [2][3].

39

### 40 **1.1 Thermal decomposition of PMCs**

41 To better understand the changes in the thermal and mechanical behaviors of polymer-based composites  
42 under fire exposure the first step usually is to investigate the influence of thermal heat fluxes, hence  
43 temperature, resulting from a fire. Such heat fluxes lead to significant temperature gradients within  
44 composite structures. From thermal analyses it is therefore possible to study the decomposition  
45 mechanisms as well as their kinetics under different testing conditions (heating rate, isothermal and  
46 anisothermal, inert or oxidizing atmosphere). The decomposition mechanisms are closely associated with  
47 the chemical nature of the polymer [4]. These analyses are extremely useful for determining the primary  
48 steps of the decomposition:  $T_d=T_{5\%}$  refers to pyrolysis or decomposition onset and corresponds to the  
49 temperature at which 5% of the polymer mass has decomposed;  $T_{max}$  refers to the maximum peak of  
50 decomposition rate. Such analyses can also be considered for studying the thermal decomposition kinetics.  
51 From a general standpoint, the influence of temperature on PMCs properties can be investigated  
52 considering two temperature ranges: (i)  $T < T_d$  and (ii)  $T > T_d$ .

53 When  $T < T_d$ , the first consequence of a temperature increase is the thermal expansion of the specimen [1].  
54 High temperature gradients and the difference in thermal expansion coefficients of the fiber and of the  
55 matrix may result in incompatibilities of deformations, leading to the appearance of matrix cracks that  
56 contribute to slowing down thermal conduction. The changes in matrix state (glass transition, melting)  
57 require energy input which can result in a slowing of the temperature increase by surface or within the  
58 sample [5]. These transformations lead to matrix softening and can promote material damage such as  
59 porosities which will induce matrix cracks, inter and intra-laminar, leading to delamination. Ancillary  
60 mechanisms, such as the formation of water vapour in matrices with high water recovery, can also damage  
61 the material via the formation and growth of porosities.

62 When  $T > T_d$ , temperature is high enough to induce thermal decomposition and damage within the  
63 material is then the most important [1]. Different chemical transformations of the material occur according  
64 to the mechanisms described in [6]. The issue of fire resistance of polymer matrices with poor temperature  
65 resistance is not widely addressed in the literature: most studies primarily focus on matrices with medium  
66 (epoxy, polyester, vinylester) or high (phenolic, PPS, PEEK) char yield [4].

67

## 68 **1.2 Thermomechanical coupling at high temperature in PMCs**

69 The influence of high temperatures on both the mechanical properties and the thermomechanical behaviour  
70 of PMCs can be considered up to  $T_d$ . In thermally stable PMCs, changes in mechanical properties with  
71 temperature can be considered reversible up to matrix decomposition [1]. In the case of a fire scenario it is  
72 necessary to consider the changes within the laminates occurring at  $T_d$  (see section 1.1). In addition, the  
73 study of the thermomechanical coupling in PMCs requires specific technical means. Such an issue has been  
74 widely addressed in the literature. As for most of the studies dealing with high temperature exposure [7], a  
75 weak coupling between thermal transfers and mechanics is postulated for our analyses. It means that the  
76 thermal state of a given point influences its mechanical behavior but a variation in its mechanical state  
77 leaves its temperature unchanged. Weak coupling refers to the influence of temperature on mechanical  
78 behaviour but not the influence of mechanical behaviour on thermal one. This section is focused on the

79 tensile behaviour under homogeneous and isothermal temperature conditions. Figure 1 shows the typical  
80 influence of temperature on the mechanical properties of PMCs under isothermal conditions (i.e. constant  
81 and uniform temperature within the material). Among the classical mechanical properties which are  
82 significantly degraded by a temperature increase, the Young's modulus, shear modulus and compressive  
83 strength are the most common ones.  $T_{cr}$  represents the critical temperature from which the properties start  
84 decreasing,  $T_g$  the glass transition temperature and  $T_m$  the melting temperature. To understand the  
85 behaviour of PMCs under critical service conditions, e.g. fire, it is necessary to determine the residual  
86 properties at temperatures higher than  $T_d$ .

87 For temperature testing conditions higher than  $T_d$ , polymer matrix decomposition may lead to a high  
88 activity of porosity formation and growth in the laminates, which severely degrades their mechanical  
89 properties and behaviour [8]. From monotonic tensile tests conducted on different types of orthotropic  
90 woven fabric laminates (glass/vinyl ester, glass/polyester and glass/polypropylene) up to 400°C (e.g. lower  
91 than  $T_d$ ), there is significant tensile strength retention at high temperatures due to the mechanical load  
92 borne by the 0° fibers [9]. To the authors' best knowledge; there are very few studies in the literature  
93 dealing with the mechanical behaviour under fire conditions [9-10]. Gibson et al. showed that the same  
94 mechanism appeared to control the failure in tension and compression (associated with the matrix melting)  
95 in TP-based composites (glass fibre reinforced PP laminates). In the case of creep loadings, the evolution of  
96 the creep stress at failure as a function of exposure time has been studied in composite materials with TP  
97 [9-10] and thermosetting (TS) [11] matrices. These studies highlight that damage mechanisms significantly  
98 depend on the applied creep stress as well as the testing temperature.

99

### 100 **1.3 Objectives of the study**

101 Before studying the coupling between thermal and mechanical behaviours in TP-based composites  
102 laminates, it is necessary to determine the characteristic temperatures ( $T_g$ ,  $T_m$ ,  $T_d$ ). Thus TGA tests were  
103 carried out under anisothermal conditions and different atmospheres (inert or oxidizing) to investigate the

104 influence of temperature on the thermal decomposition of C/PPS composite and its constitutive materials.  
105 From the knowledge of the characteristic temperatures, it is therefore possible to conduct mechanical tests  
106 (monotonic tension and tensile creep) under isothermal conditions to specifically address the issue of  
107 thermomechanical coupling within carbon fibers reinforced PPS laminates for testing temperatures ranging  
108 from ambient temperature to temperatures higher than  $T_d$ .

109

## 110 **2. Material and methods**

### 111 **2.1 Materials and specimens**

112 The studied composite materials are carbon fabric reinforced laminates consisting of a semi-crystalline  
113 high-performance PPS supplied by the Ticona company. The woven-ply prepreg, supplied by SOFICAR,  
114 consists of 5-harness satin weave carbon fiber fabrics (T300 3K 5HS) whose weight fraction is 58%. The  
115 prepreg plates are hot pressed according to a quasi-isotropic [(0,90)/(±45)/(0,90)/(±45)/(0,90)/(±45)/(0,90)]  
116 stacking sequence. The glass transition temperature of the material is  $T_g=98^\circ\text{C}$  and its melting temperature  
117  $T_m=280^\circ\text{C}$ , as measured by DSC [12]. The degree of crystallinity of PPS matrix is close to 30% and the  
118 initial porosity ratio is very small (less than 2%).

119

### 120 **2.2 Experimental set-up**

#### 121 **2.2.1 Thermogravimetric Analysis (TGA)**

122 To carry out these experiments a thermo-gravimetric analyzer TA Instruments Discovery is used. Thermal  
123 decomposition is characterized under three atmospheres: nitrogen, air and dioxygen. The gas flow rate is  
124 set at  $20 \text{ mL}\cdot\text{min}^{-1}$ . The extent of decomposition is characterized by a degree of progress in the reaction  
125 defined by the following expression [13]:

$$126 \quad \alpha = \frac{m_i - m}{m_i - m_f} \quad (1)$$

127 With  $m_i$  the initial mass of the sample,  $m$  is the mass at a time  $t$  and  $m_f$  is the mass after decomposition.

128 When the analysis is carried out in an inert atmosphere,  $\alpha$  corresponds to the degree of pyrolysis and its

129 value reaches 1 for a fully completed pyrolysis. Under oxidizing atmosphere, it corresponds to the degree  
130 of decomposition and its value is 1 when the entire solid residue is completely gasified.

131 The thermal decomposition of studied materials (Plain PPS resin and C/PPS composite) has been  
132 conducted using anisothermal heating at 10°C/min from room temperature to 700°C. These experiences are  
133 supposed to be representative of the increase in material temperature during the transient phase of its  
134 thermal response. However they are not suitable for clearly identifying the involved chemical mechanisms.  
135 These analyses were conducted on samples whose initial mass is about 8mg.

136

### 137 **2.2.2 Porosities rate via density measurements**

138 The density of solids can be determined using the buoyancy method. The density is determined using  
139 Archimedes' Principle. The upward buoyant force exerted on a body immersed in a fluid is equal to the  
140 weight of the fluid the body displaces. Density determination using the buoyancy method is based on the  
141 following formula [14]:

$$142 \quad \rho = \rho_{fl} * \frac{w_a}{(w_a - w_{fl})} \quad (2)$$

143 Where  $\rho$  is the density of sample,  $\rho_{fl}$  is the density of buoyancy liquid,  $w_a$  is the weight of sample in air and  
144  $w_{fl}$  is the weight of sample in liquid. The density is determined by means of a densitometry balance  
145 Sartorius Secura whose accuracy is 1mg.

146 Finally, the porosity rate or void fraction is therefore defined from the density of sample as follows:

$$147 \quad P = 1 - \frac{\rho}{\rho_0} \quad (3)$$

148 Where  $\rho_0$  is the density of the sample referred to as-received.

149 Specimens whose dimensions are 25\*25\*2.2mm where subjected to isothermal temperature conditions  
150 (465-500-530°C) for different exposure times (5-10-20-30-40-60 min) in a primary vacuum furnace to  
151 evaluate the changes in the residual mass associated with thermal decomposition. Specimens are put into  
152 the furnace once the temperature is stabilized.

### 153 2.2.3 Tensile mechanical testing under isothermal conditions

154 The tensile mechanical behaviour under isothermal conditions is investigated using a uniaxial servo-  
155 hydraulic machine MTS, equipped with hydraulic grips and a load cell with a 100kN capacity. Stable and  
156 homogeneous temperature conditions are applied by means of a tube furnace composed of 3 zones, which  
157 is positioned between the grips of the machine. High temperature testing conditions (e.g. temperatures  
158 close to or higher than polymer matrix decomposition temperature) usually requires samples with a specific  
159 geometry because temperatures are sometimes beyond the range of testing ovens. In the present case, the  
160 dimensions of the tube furnace make it necessary to use specimens with a gage length of 20cm long (Fig.  
161 2). The tensile mechanical properties were determined according to the European standards EN 6035 [15].  
162 The axial modulus ( $E_x$ ) and ultimate strength ( $\sigma^u$ ) were calculated from the following definitions:

$$163 \quad E_x = \frac{\Delta F}{S \cdot \Delta \varepsilon_x} \quad \text{and} \quad \sigma^u = \frac{F^u}{S} \quad (1)$$

164 Where  $\Delta F$  is the difference in the tensile loads at  $(\varepsilon_x)_2 = 0.25\%$  and  $(\varepsilon_x)_1 = 0.05\%$ ,

165  $S$  is the specimen cross section,

166  $\Delta \varepsilon_x = (\varepsilon_x)_2 - (\varepsilon_x)_1$  is the difference in the axial strains obtained from the cross machine  
167 displacement,

168  $F^u$  is the maximum force borne by the specimen at failure.

169

### 170 Estimation of the axial stiffness under different isothermal conditions

171 The evolution of the axial stiffness  $E_x$  with temperature was measured from the following experimental  
172 protocol:

- 173 • Heating to a temperature T1 at 50°C/min,
- 174 • Two minutes at T1 (to ensure the temperature homogeneity through-the-thickness),
- 175 • Mechanical loading (50 MPa) then unloading at 0 MPa,
- 176 • Measurement of axial stiffness during unloading (the low viscosity of the matrix can cause the  
177 extensometer to slip during loading),

178 The testing temperatures range from ambient temperature to 520°C.



179 **Tensile response to failure under different isothermal conditions**

180 The monotonic tensile behavior at failure was investigated under different isothermal conditions. As for  
181 stiffness measurements, the specimens are heated to 50°C/min and then maintained at the test temperature  
182 for 2 minutes to ensure homogeneity of the temperature through-the-thickness. The tensile test is conducted  
183 in cross machine displacement-controlled mode at a rate of 2 mm.min<sup>-1</sup>. The ultimate tensile strength and  
184 tensile behaviour have been studied for temperatures representative of four different material states:

- 185 • 220°C: rubbery state of the PPS matrix between T<sub>g</sub> (Glass transition) and T<sub>m</sub> (Melting),
- 186 • 270°C: slightly melted material,
- 187 • 320°C: completely melted material,
- 188 • 470°C: slightly decomposed material.

189

190 **Tensile creep behavior under isothermal conditions**

191 Finally, creep tests were performed on quasi-isotropic C/PPS specimens according to the following  
192 experimental protocol:

- 193 • Tensile mechanical loading (loading time = 10 seconds)
- 194 • Temperature increase from room temperature to 320°C at a rate of 25°C.min<sup>-1</sup>. This temperature is  
195 selected because the failure behaviour at this temperature has been characterized in the case of  
196 monotonic tensile tests.
- 197 • Both mechanical loading and temperature level (320°C) are maintained.

198 It has been chosen to apply the mechanical force first and then the temperature increase because it  
199 corresponds to the succession of solicitations an in-service material would have to face in the event of fire.

200 At the laboratory scale, a mechanically loaded sample is suddenly subjected to a heat flux applied by means  
201 of a tube furnace. The creep levels tested vary between 8 and 31% of the ultimate strength  $\sigma_u$  at ambient  
202 temperature). These stress levels are chosen such as to analyze the tensile behavior for tensile loadings  
203 lower and higher than the onset of necking.

### 204 3. Results and discussion

#### 205 3.1 TGA tests

206 Before considering mechanical testing under different isothermal conditions, it is utmost important to  
207 investigate the thermal decomposition of plain PPS matrix and C/PPS laminates by means of TGA tests  
208 under anisothermal conditions and different atmospheres (inert and oxidizing), with a particular attention  
209 paid to the determination of decomposition temperature [16-17]. An inert atmosphere is representative of  
210 what specimens undergoes at core with respect to what specimens experience in an oxidizing atmosphere at  
211 the outer surface.

212 Under dioxygen, the thermal decomposition of PPS begins at 502°C, approximately the same temperature  
213 as under an inert atmosphere (see Table 1). The curve representing the Mass Loss Rate (MLR) of plain PPS  
214 resin as a function of temperature  $MLR = f(T)$  is characterized by 3 peaks (see Figure 3). The first peak  
215 corresponds to a mass loss of about 15%. Thus it may be associated with the first pyrolysis mechanism,  
216 depolymerization (Figure 4b). Following this reasoning, the second peak, which extends to  $\Delta m = 37\%$ ,  
217 may be associated with the second pyrolysis mechanism. Even before the pyrolysis ends a new mechanism  
218 starts and may be associated with the simultaneous oxidation of PPS matrix and the pyrolysis residue as it  
219 extends until the entire initial material is carbonated (Figure 4a). The maximum oxidation rate is virtually 3  
220 times higher than the pyrolysis rate.

221 The decomposition of carbon fibre-reinforced composites under oxidizing atmosphere is faster than the one  
222 of other fibers-reinforced composites (e.g. glass fibers), because carbon fibres are sensitive to oxidation  
223 phenomena just like polymeric matrices. For practical reasons decomposition under air has been little  
224 studied, as the oxidation phenomena are mainly characterized with TGA analyses under dioxygen. In  
225 C/PPS, thermal decomposition under air begins at 517°C compared to 483 and 515°C under N<sub>2</sub> and O<sub>2</sub>  
226 respectively (see Table 1). Thus the mechanisms of crosslinking and improvement of thermal resistance  
227 observed under O<sub>2</sub> do not appear to occur under air. Oxidation appears to start faster under O<sub>2</sub> simply  
228 because there are more reactive species and the atmosphere is more oxidizing.

229 Similar observations have already been made by Ma et al. in the study of the decomposition of C/PPS  
230 under air [18]. When heated in an oxidizing atmosphere at temperatures higher than its melting  
231 temperature, PPS can crosslink like a thermosetting polymer thus having a higher thermal stability. If the  
232 delay in the onset of decomposition is only observed in C/PPS composite, this suggests that these  
233 phenomena are promoted by the presence of fibres. As for plain PPS resin pyrolysis and char oxidation  
234 overlap in the C/PPS. Nevertheless the fact that the second peak of MLR ends with a mass loss of 43%  
235 equivalent to the matrix mass in the composite, it tends to indicate that oxidation of char and fibres occurs  
236 separately and not simultaneously (Figure 4).

237 Under air, the thermal decomposition of PPS begins at 508°C. For the same heating rate, decomposition  
238 begins at 503°C and 502°C respectively under N<sub>2</sub> and O<sub>2</sub> (see Table 1). Pyrolysis results in a mass loss of  
239 39%, which is lower than that observed under inert atmosphere (Figure 5a), which is consistent with the  
240 observations made in the case of a PEEK resin by Patel et al [19-20]. As under dioxygen, oxidation begins  
241 before the pyrolysis ends. Nevertheless the appearance of the characteristic peak of pyrolysis on the MLR  
242 curve  $MLR = f(T)$  indicates that pyrolysis is almost completed when oxidation begins under air (Figure 5b)  
243 while it did not even reach its maximum rate when this transition occurs under O<sub>2</sub>.

244

### 245 **3.2 Determination of porosity rate as a function of the degree of decomposition**

246 C/PPS laminates specimens undergo different degrees of thermal decomposition when they are subjected to  
247 isothermal conditions for different exposure times in a primary vacuum furnace (oxidizing atmosphere).  
248 Three temperature levels (465-500-530°C) and 6 exposure times (5-10-20-30-40-60 min) were considered  
249 to induce changes in the residual mass associated with thermal decomposition. From the evaluation of the  
250 residual mass it is therefore possible to assess the changes in the degree of decomposition vs time  
251 according to Eq. (1), as well as the porosity rate vs time with Eq. (2) and (3). Figure 6a represents the  
252 evolution of specimens' residual mass as a function of the exposure time at given temperatures. The initial  
253 decrease in the residual mass is all the more significant than the testing temperature is elevated. As a  
254 consequence, the degree of decomposition ranges from 50 to 80% after a 5 minutes exposure (Fig. 6b). The

255 transient stage lasts about 10 minutes before the mass loss and the degree of decomposition reach a  
256 stationary state (Fig. 6). During the transient stage, the higher the test temperature, the higher the thermal  
257 decomposition rate is contrary to what is observed during the stationary stage. After a 40 minutes exposure,  
258 all the curves representing the degree of decomposition vs time converge, suggesting that regardless the  
259 testing temperatures, the differences in the thermal decomposition kinetics ultimately result in the same  
260 degree of decomposition. Finally, figure 7 represents the porosity rate as a function of the degree of  
261 decomposition for the different testing temperatures. It appears that all the experimental points virtually  
262 follow the same evolution to reach a plateau corresponding to about 35% of porosities within the  
263 specimens. From these curves, one can assume that the porosities rate is very well correlated with the  
264 degree of decomposition. The knowledge of the porosities rate is important as porosities within the  
265 laminates are stress concentrators contributing to the degradation of the mechanical properties.

266

### 267 **3.3 Tensile mechanical testing under isothermal conditions: monotonic loading**

268

#### 269 **3.3.1 Evolution of axial stiffness with temperature**

270 The evolution of the axial stiffness under different isothermal conditions is shown in Figure 8. The material  
271 initially loses 14% of its axial stiffness when testing temperature becomes higher than the glass transition  
272 temperature of the PPS matrix (about 98°C, see section 2.1). This decrease may be attributed to the  
273 decrease in the shear modulus of the  $\pm 45^\circ$  plies during softening of the matrix (-67% at Tg [21]). Above the  
274 glass transition temperature, the axial stiffness of the laminate decreases gradually up to 220°C. This  
275 phenomenon is associated with the decrease in shear strength of the PPS matrix and the fibre-matrix  
276 interface as the viscosity of the matrix increases.

277 There is a significant drop in axial stiffness for a temperature taken between 220 and 270°C. This can be  
278 linked to the melting of the matrix ( $T_m=280^\circ\text{C}$ , see section 2.1) and the significant degradation of the fiber-  
279 matrix interface. Indeed, according to the results of DSC [12], the melting occurs between 220 and 295°C  
280 (even if the shape of the melting peak suggests that most of the crystalline zones are destroyed around  
281 280°C). After melting, the  $\pm 45^\circ$  plies no longer play a mechanical role because their behaviour is driven by

282 the matrix. Beyond that temperature, the material has a residual stiffness equal to 58% which comes solely  
283 from the contribution of 0/90° oriented plies. The latter initially bear 73% of the load (according to  
284 laminate theory), the decrease in their stiffness after melting can be estimated at 19%. These observations  
285 are in agreement with the results obtained by Mahieux et al. on a C/PPS laminate [22]. Thus, the stiffness  
286 reductions of constitutive elements considered individually do not explain the decrease with temperature  
287 observed in the C/PPS composite laminates. The PPS has a stiffness 100 times lower than that of the  
288 carbon fibres, which virtually retain their initial stiffness at this temperature level. The decrease in the  
289 stiffness of the 0/90° plies may result from other damage mechanisms such as the appearance of transverse  
290 cracks at the interface between strands and matrix. These mechanisms are suspected to take place mainly at  
291 the overlap areas of the longitudinal and transverse strands as a consequence of the stress concentration  
292 induced by longitudinal strands (mechanically loaded) on the transverse strands (Fig. 9), as well as  
293 metadelamination.

294 Above the melting temperature, the axial stiffness no longer changes, at least until 520°C (maximum  
295 temperature studied). When the ±45° plies have lost all rigidity after PPS melting, the axial stiffness of the  
296 material is mainly due to the stiffness carbon fibres parallel to the loading direction, which is virtually  
297 unchanged up to 1000-1400°C (depending on the fibres) in an inert atmosphere [23]. Then the longitudinal  
298 stiffness of the composite is assumed to be virtually unchanged up to these temperatures, unless fibres  
299 undergo oxidation. However these assumptions cannot be confirmed here because the behaviour of C/PPS  
300 could not be characterized for temperatures higher than 520°C due to the ignition of pyrolysis gases into  
301 the tube furnace.

302

### 303 **3.3.2 Tensile response to failure under different isothermal conditions**

304 Figure 10 shows the influence of different isothermal conditions on the tensile response of quasi-isotropic  
305 C/PPS laminates whose mechanical behavior is fibre-dominated. The ultimate tensile strength dramatically  
306 decreases (about 25% of its initial value – see Table 2) between room temperature to 470°C (lower than the  
307 onset decomposition temperature). At 220°C, the material exhibits a quasi-linear behaviour with a bending

308 at around 180 MPa (referred to as knee point in the literature [24]) characteristic of matrix cracking, which  
309 occurs most frequently in overlapping areas of strands (Figure 9a). The catastrophic failure is driven by the  
310  $0^\circ$  fibres whose elongation at failure is significantly lower than the PPS matrix one. The observation of  
311 specimens surfaces show a womb type failure surface resulting from the poor adhesion of the fibre-matrix  
312 interface, which is often observed in composites with thermoplastic matrices. This poor adhesion is  
313 promoted by the high temperatures and low viscosity of the matrix (Fig. 11).

314 At  $270^\circ\text{C}$ , the behaviour remains generally elastic-fragile, with a noticeable inflection around 25 MPa. This  
315 non-linearity is associated with the localized crushing of the strands in the overlap area, which first results  
316 in: (i) deformation localization in resin-rich areas and (ii), only then, in matrix cracking. On the front and  
317 rear faces of the specimens, the surface crack densities is more important than at  $220^\circ\text{C}$  (Fig. 9b). The  
318 ultimate stress is between 2 and 3 times lower than at  $220^\circ\text{C}$  and the elongation at failure is about 20%  
319 lower, which means that damage can also be explained by the higher density of inter- and intra-laminar  
320 cracks than at  $220^\circ\text{C}$  (Fig. 12).

321 For temperatures higher than  $T_m$ , significant changes in the mechanical response are observed. Before  
322 melting, the fibres of the same strand are held by the matrix and elongate evenly within the strand. After  
323 melting, the cohesion of the strand is no longer insured by the matrix, allowing significant transverse  
324 contraction of the fibres and a more significant elongation. Thus, for stresses higher than 70 MPa, the  
325 elongation of the  $0^\circ$  strands is accompanied by the generalization of the necking along the  $0^\circ$  direction.  
326 This necking ultimately results in a generalized necking of the  $90^\circ$  oriented plies, which greatly increases  
327 the bending force at the crimp (where the warp strands undulate over the weft strands) and leads to the  
328 misalignment of the strands (Fig. 13a).

329 Beyond a certain elongation, the generalization of necking is such that the transverse strands are strongly  
330 crushed by the longitudinal strands. Such crushing leads to significant out-of-plane displacements resulting  
331 in surface bending effects and extensive delamination (Fig. 14). In  $\pm 45^\circ$  plies, the fusion of the matrix is  
332 accompanied by a reorientation of the strands in the direction of sollicitation. They then undergo a shear  
333 stress at the level of their overlapping areas. The space between the strands decreases until they enter the

334 contact, causing the rotation to be blocked and their transverse contraction to begin [25]. The transition  
335 between the two phenomena (reorientation and compaction) is characterized as follows by a “shear  
336 locking” angle. When the specimen is elongated, the compaction increases and results in the stiffening of  
337 rotation of  $\pm 45^\circ$  plies leading to the increase in laminates axial stiffness.

338 For temperatures higher than  $T_m$ , the actual failure of the specimens could not be observed. Indeed, the  
339 necking of  $0^\circ$  strands extends along the  $0^\circ$  direction until it reaches the area of the specimen taken in the  
340 machine grips. Necking generalization is associated with an elongation of approximately 40% and a  
341 significant reduction (about 25%) in their initial diameter (Fig. 13b). Tensile tests suggest that both  
342 deformation and damage mechanisms significantly change in C/PPS laminates subjected to monotonic  
343 loading at temperatures higher than PPS matrix melting temperature. However, creep loadings are more  
344 representative of the critical service conditions met by mechanically loaded composite parts exposed to a  
345 fire scenario. From the tensile failure behaviour of C/PPS laminates investigated in this section, significant  
346 changes in the monotonic thermomechanical behaviors are observed at temperatures higher than  $T_m$ . In  
347 quasi-isotropic C/PPS laminates whose mechanical behaviour is driven by  $0^\circ$  plies, the rate-dependent  
348 behaviour is very limited at temperatures lower than  $T_m$  [26], but it is expected to be much more important  
349 at temperatures higher than  $T_m$ .

350

### 351 **3.3.3 Tensile mechanical testing under isothermal conditions: creep loading**

352 The evolution of time to failure as a function of tensile creep stress is shown in Figure 15. The time to  
353 failure corresponds to the time elapsed since the application of mechanical loading. **The time to failure**  
354 **significantly decreases as creep stress increases. As a result, three specific failure mechanisms have been**  
355 **identified in C/PPS laminates under creep loading depending on the applied creep stress:**

- 356 • For a creep stress higher than  $0.25\sigma_u$ , the failure occurs even before the material reaches its  
357 melting temperature. On the one hand, the failure therefore results from the decrease in the  
358 mechanical strength of the  $\pm 45^\circ$  plies (related to matrix softening and degradation of the  
359 fiber/matrix interface). On the other hand, it is associated with the appearance of transverse cracks

360 and meta-delamination in 0/90° oriented plies (Fig. 9a and 12a). The failure mechanism is similar  
361 to that observed in figure 11, i.e. a transverse break of the fibres at 0°.

362 • For intermediate creep stresses ( $0.11\sigma_u \leq \sigma_{creep} \leq 0.15\sigma_u$ ), failure occurs at the beginning of the  
363 creep test or in some cases shortly before the material has reaches 320°C. Thus, the failure can be  
364 associated with matrix melting and damage mechanisms similar to those observed during tensile  
365 tests at 320°C. The creep stress is then approximately equivalent to the one for which necking  
366 starts at 320°C (Fig. 10). The creep stress being higher than the stress levels where necking occurs  
367 in monotonous tensile tests, the deformation mechanisms that occur at that time (elongation of the  
368 longitudinal strands and crushing of transverse strands in 0/90° plies, reorientation of  $\pm 45^\circ$  plies)  
369 will be initiated and developed within a few seconds, resulting in a deformation of the specimen  
370 without reaching ultimate failure, in agreement with the mechanisms observed during monotonous  
371 tension (Fig. 13b).

372 • For a stress lower than 60 MPa, there is an increase in the elongation of the specimen as  
373 temperature increases, but once 320°C is reached, the deformation no longer evolves. Indeed,  
374 despite matrix melting, the applied stress is too low to initiate necking.

375

#### 376 **4. Conclusion**

377 In the literature, there are very few studies dealing with the mechanical behaviour of thermoplastic matrix  
378 composite materials beyond matrix melting temperature  $T_m$ . Through the results and discussion proposed in  
379 the present work, melting and thermal decomposition are instrumental to rule the tensile behavior of quasi-  
380 isotropic C/PPS laminates. Between the ambient temperature and  $T_m$ , the laminates axial stiffness decreases  
381 with increasing temperature, mainly due to the loss of stiffness of the  $\pm 45^\circ$  oriented plies and the  
382 degradation of the fibre-matrix interface. Beyond  $T_m$ , the axial stiffness no longer changes, as long as no  
383 oxidation takes place. Conversely, matrix melting significantly influences the damage mechanisms within  
384 the laminate. The bonding of carbon fibres within the strands is no longer ensured, and the 0° strands  
385 experience necking resulting in a much higher elongation than the one observed before matrix melting.  
386



387 This elongation comes along with other phenomena such as the reorientation of the  $\pm 45^\circ$  plies and the  
388 crushing of transverse strands that are not observed before melting. Finally, for testing temperatures close  
389 to the onset decomposition temperature, porosities appear and grow within the laminates. The porosities  
390 rate is very well correlated with the degree of decomposition. The knowledge of porosities rate is utmost  
391 important as they are stress concentrators contributing to the degradation of the mechanical properties.

392

393

#### 394 **References**

395 [1] A.P. Mouritz, A.G. Gibson. Fire properties of polymer composite materials. N° 143 Solid mechanics  
396 and its applications. Springer, Dordrecht, 2006.

397 [2] T.N.A. Browne. A model for the structural integrity of composite laminates in fire. PhD doctoral  
398 dissertation, University of Newcastle upon Tyne, 2006.

399 [3] A.G. Gibson, M.E.O. Torres, T.N.A. Browne, S. Feih, A.P. Mouritz. High temperature and fire  
400 behaviour of continuous glass fibre/polypropylene laminates. Composites Part A: Applied Science and  
401 Manufacturing, 41(9):1219–1231, 2010.

402 [4] B. Vieille, A. Coppalle, C. Keller, M.-R. Garda, Q. Viel, E. Dargent. Correlation between post fire  
403 behavior and microstructure degradation of aeronautical polymer composites. Materials and Design 2015;  
404 74:76–85.

405 [5] A. Atreya et S. Agrawal : An experimental and theoretical investigation into burning characteristics of  
406 PPS-glass fiber composites. In 8th AIAA/ASME joint thermophysics and heat transfer conference, 2002.

407 [6] D. Drysdale. An introduction to fire dynamics. John Wiley & Sons, 2011.

408 [7] C. Mercadé : Modélisation de la dégradation d'un matériau composite carbone-époxy soumis à une  
409 sollicitation thermo-mécanique couplée. Application aux réservoirs d'hydrogène de type IV. Thèse de  
410 doctorat, Ecole Nationale Supérieure de Mécanique et d'Aérotechnique Chasseneuil-du-Poitou, 2017.

411 [8] R.L. Coble and W.D. Kingery. Effect of porosity on the physical properties of sintered alumina. Journal  
412 of the American Ceramic Society, 1956; 39:381.

- 413 [9] T.N.A. Browne, Fire Behaviour of Composite Laminates, Ph.D. thesis, University of Newcastle upon  
414 Tyne, 2006.
- 415 [10] A. G. Gibson, M. E. O. Torres, T. N. A. Browne, S. Feih et A. P. Mouritz : High temperature and fire  
416 behaviour of continuous glass fibre/polypropylene laminates. *Composites Part A : Applied Science and*  
417 *Manufacturing*, 41(9):1219–1231, 2010.
- 418 [11] S. Feih, Z. Mathys, A. G. Gibson et A. P. Mouritz : Modelling the compression strength of polymer  
419 laminates in fire. *Composites Part A : Applied Science and Manufacturing*, 38(11):2354–2365, 2007.
- 420 [12] D. Blond, B. Vieille, M. Gomina, L. Taleb. Correlation between physical properties, microstructure  
421 and thermo-mechanical behavior of PPS-based composites processed by stamping. *Journal of Reinforced*  
422 *Plastics and Composites* 2014; 33(17): 1656-1668.
- 423 [13] J.H. Flynn. The historical development of applied nonisothermal kinetics. In *Thermal Analysis*,  
424 Volume 2, pages 1111–1126. R.F. Schwenker and P.D. Garn, New York, 1969.
- 425 [14] B. Madsen, H. Lilholt. Physical and mechanical properties of unidirectional plant fibre composites - an  
426 evaluation of the influence of porosity, *Composites Science and Technology* 2003, 63(9): 1265-1272.
- 427 [15] Test standard EN 6035, Aerospace series - Fiber-reinforced plastics - Test Method. Determination of  
428 notched and unnotched tensile strength Published by the European Association of Aerospace Industries  
429 (AECMA), april 1996.
- 430 [16] S. Feih, A. P. Mouritz. Tensile properties of carbon fibres and carbon fibre–polymer composites in  
431 fire. *Composites Part A : Applied Science and Manufacturing* 2012, 43(5):765–772.
- 432 [17] P. Tadini, N. Grange, K. Chetehouna, N. Gascoïn, S. Senave, I. Reynaud. Thermal degradation  
433 analysis of innovative PEKK-based carbon composites for high-temperature aeronautical components.  
434 *Aerosp Sci Technol* 2017; 65:106–16. doi:10.1016/j.ast.2017.02.011.
- 435 [18] C.-C.M. Ma, H.-C. Hsia, W.-L. Liu, J.-T. Hu. Studies on Thermogravimetric Properties of  
436 Polyphenylene Sulfide and Polyetherether Ketone Resins and Composites. *Journal of Thermoplastic*  
437 *Composite Materials* 1988; 1(1):39–49.

438 [19] P. Patel, T.R. Hull, R.W. McCabe, D. Flath, J. Grasmeyer, M. Percy. Mechanism of thermal  
439 decomposition of poly(ether ether ketone) (PEEK) from a review of decomposition studies. *Polymer*  
440 *Degradation and Stability* 2010; 95(5):709–718.

441 [20] P. Patel, T.R. Hull, R. E. Lyon, S.I. Stoliarov, R.N. Walters, S. Crowley, N. Safronava. Investigation  
442 of the thermal decomposition and flammability of PEEK and its carbon and glass-fibre composites.  
443 *Polymer Degradation and Stability* 2011; 96(1):12–22.

444 [21] B. Vieille, J. Aucher, L. Taleb. Influence of temperature on the behavior of carbon fiber fabrics  
445 reinforced PPS laminates. *Materials Science and Engineering: A* 2009; 517(1–2): 51-60,

446 [22] C. A. Mahieux et K. L. Reifsnider : Property modeling across transition temperatures  
447 in polymers : application to thermoplastic systems. *Journal of Materials Science*, 37:911–920, 2002.

448 [23] C. Sauder : Relation microstructure/propriétés à haute température dans les fibres et matrices de  
449 carbone. Thèse de doctorat, Bordeaux 1, 2001.

450 [24] T. Osada, M. Mizoguchi et M. Kotaki : Initial micro fracture behavior of woven fabric composites. In  
451 *Proceedings of the 13th International Conference on Composite Materials*, Beijing, 2001.

452 [25] S.V. Lomov, Ph. Boisse, E. Deluycker, F. Morestin, K. Vanclooster, D. Vandepitte, I. Verpoest et A.  
453 Willems : Full-field strain measurements in textile deformability studies. *Composites Part A : Applied*  
454 *Science and Manufacturing*, 39(8):1232–1244, 2008.

455 [26] W. Albouy, B. Vieille, L. Taleb, Experimental and numerical investigations on the time-dependent  
456 behavior of woven-ply PPS thermoplastic laminates at temperatures higher than glass transition  
457 temperature. *Composites Part A: Applied Science and Manufacturing* 2013; 49: 165-178.

458

459

460 **List of figure**

461 Fig. 1 – Influence of isothermal heating on the mechanical property of PMC laminates (Adapted from [1])

462 Fig. 2 – Tensile specimens used for characterizing the mechanical behaviour of C/PPS laminates under  
463 homogeneous and isothermal temperature conditions

464 Fig. 3 – TGA tests under O<sub>2</sub>: evolution of the residual mass and the decomposition rate (MLR) of plain PPS  
465 resin and C/PPS as a function of temperature

466 Fig. 4 – Evolution of the decomposition rate under O<sub>2</sub> as a function of the mass loss

467 Fig. 5 – Thermal decomposition of the plain PPS resin and C/PPS composites: (a) Residual mass and  
468 decomposition rate (MLR) under air in as a function of temperature (b) Decomposition rate as a function of  
469 degree of decomposition

470 Fig. 6 – Study of the thermal decomposition in C/PPS laminates subjected to isothermal conditions:

471 Evolution of the residual mass (a) and the degree of decomposition (b) vs time

472 Fig. 7 – Evolution of the porosities rate vs the degree of decomposition in C/PPS laminates subjected to  
473 isothermal conditions

474 Fig. 8 – Evolution of the axial stiffness of quasi-isotropic C/PPS laminates under isothermal conditions

475 Fig. 9 – C/PPS laminates front view observations, before failure at: (a) 220°C (b) 270°C

476 Fig. 10 – Influence of temperature on the tensile response of quasi-isotropic C/PPS laminates

477 Fig. 11 – Fractographic observations of tensile failure surfaces at 220°C

478 Fig. 12 – Quasi-isotropic C/PPS laminates edge after failure: (a) 220°C - (b) 270°C

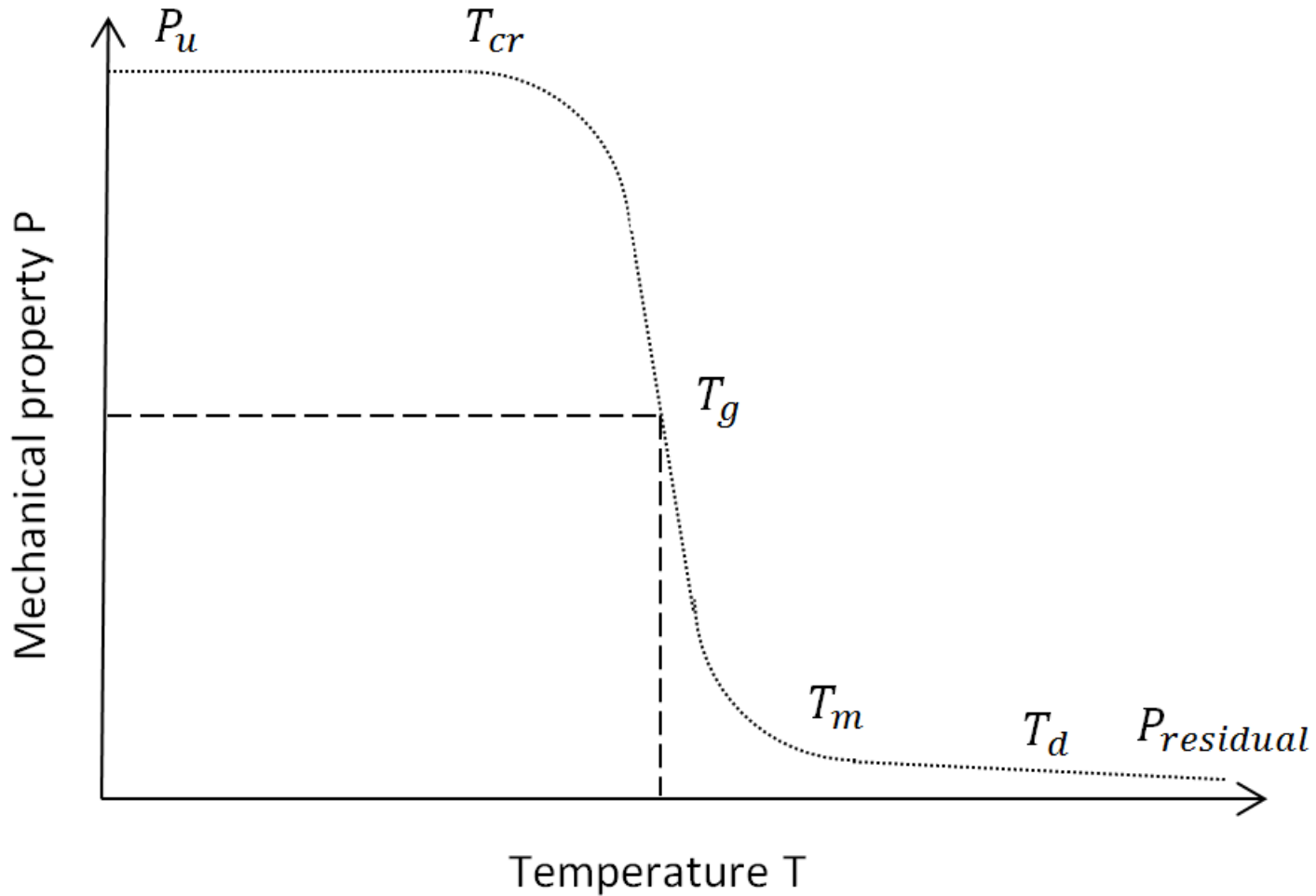
479 Fig. 13 – (a) Disalignment of transverse strands coming along with the necking along the 0° direction (b)

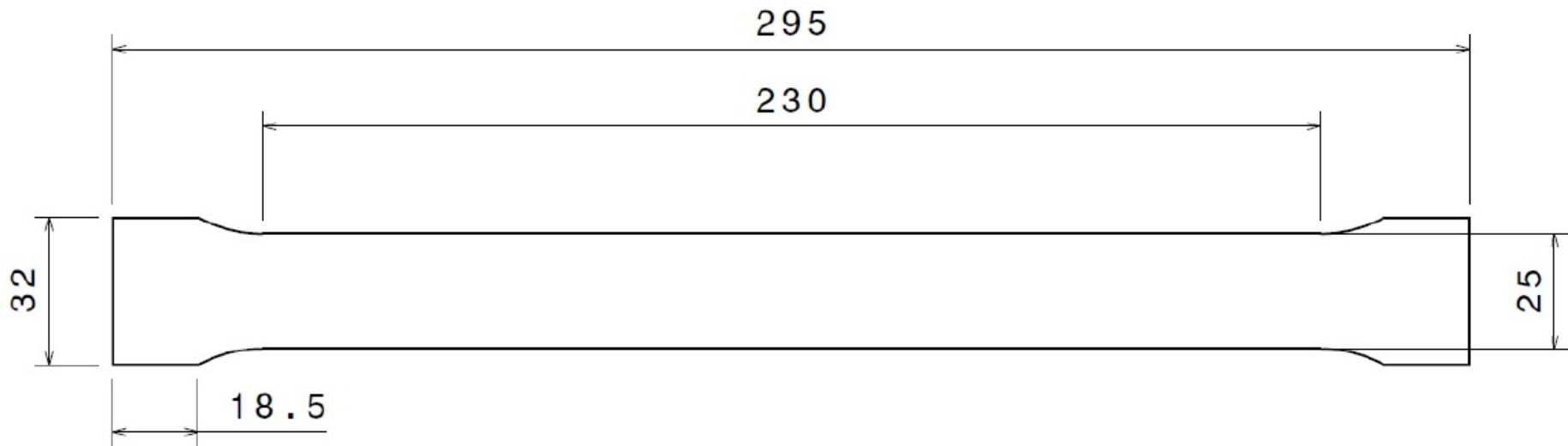
480 Generalization of necking and crushing of transverse strands (for  $T > T_m$ )

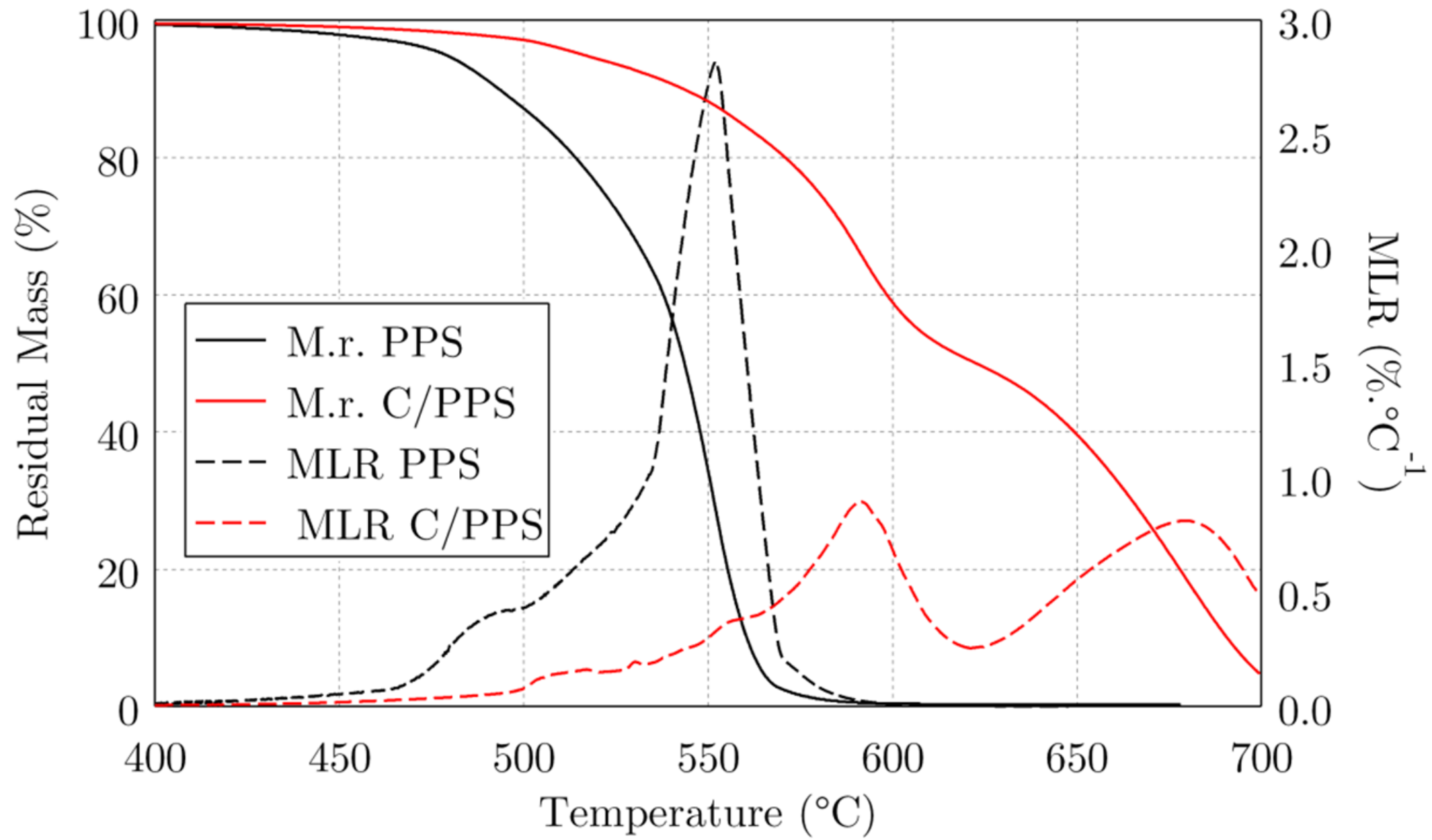
481 Fig. 14 – Quasi-isotropic C/PPS laminates edge after failure at 470°C

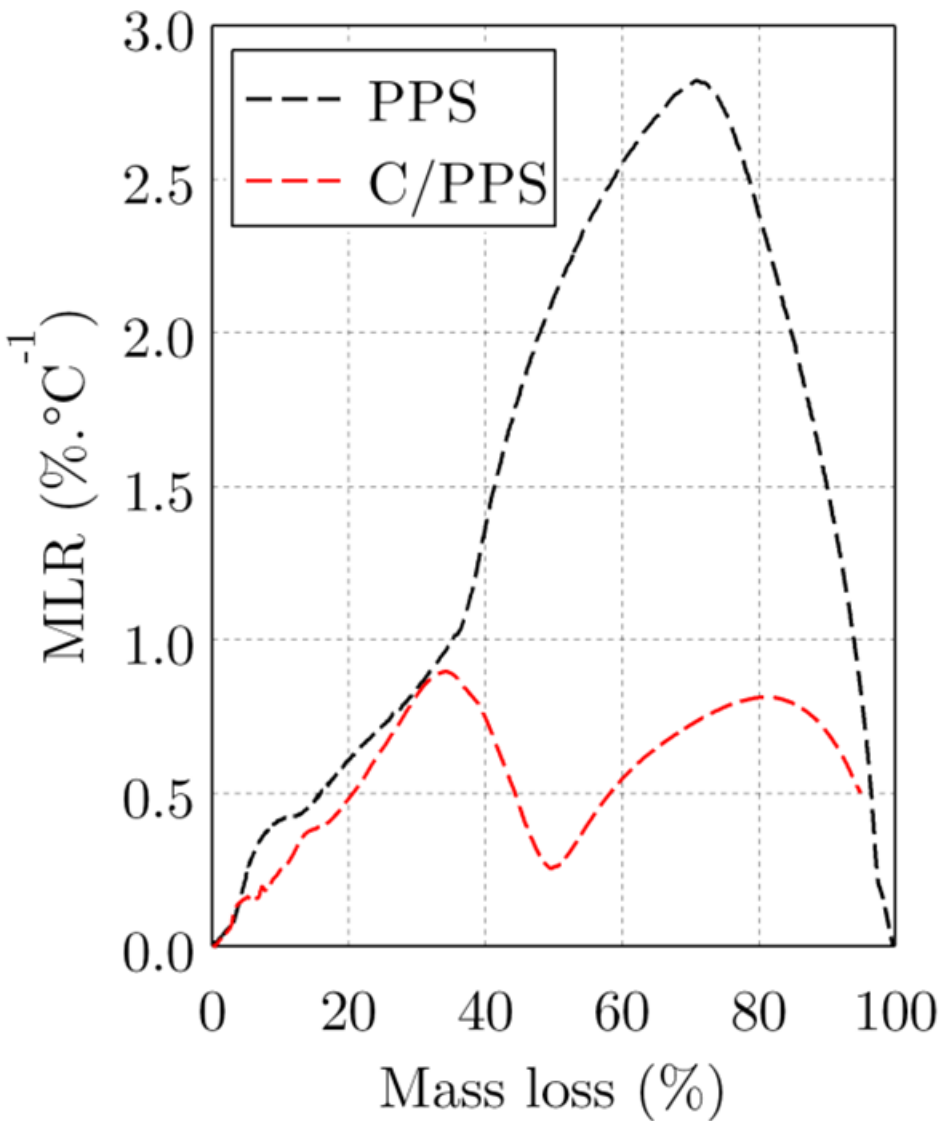
482 Fig. 15 – Creep test at 320°C: time to failure as a function of creep stress

483

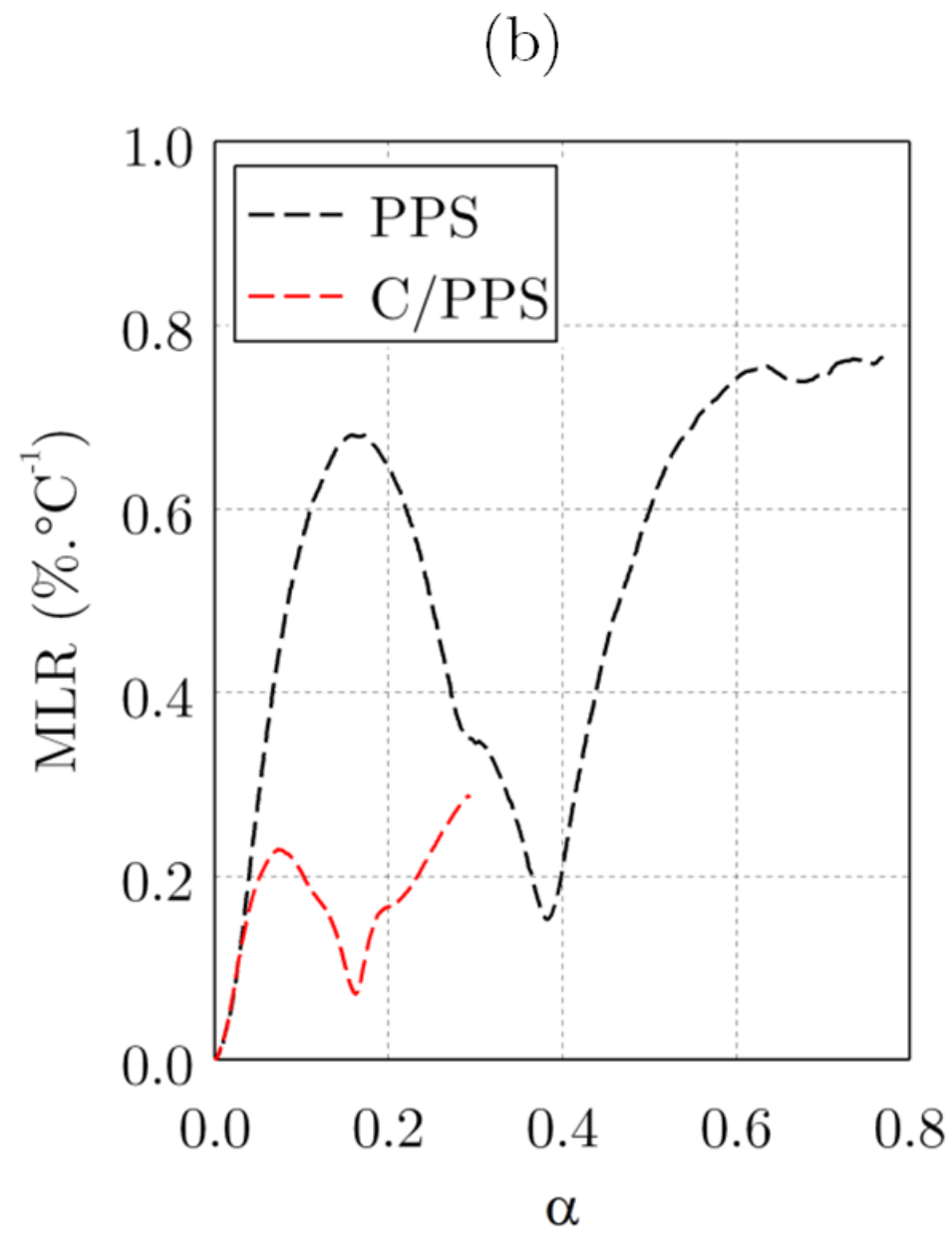
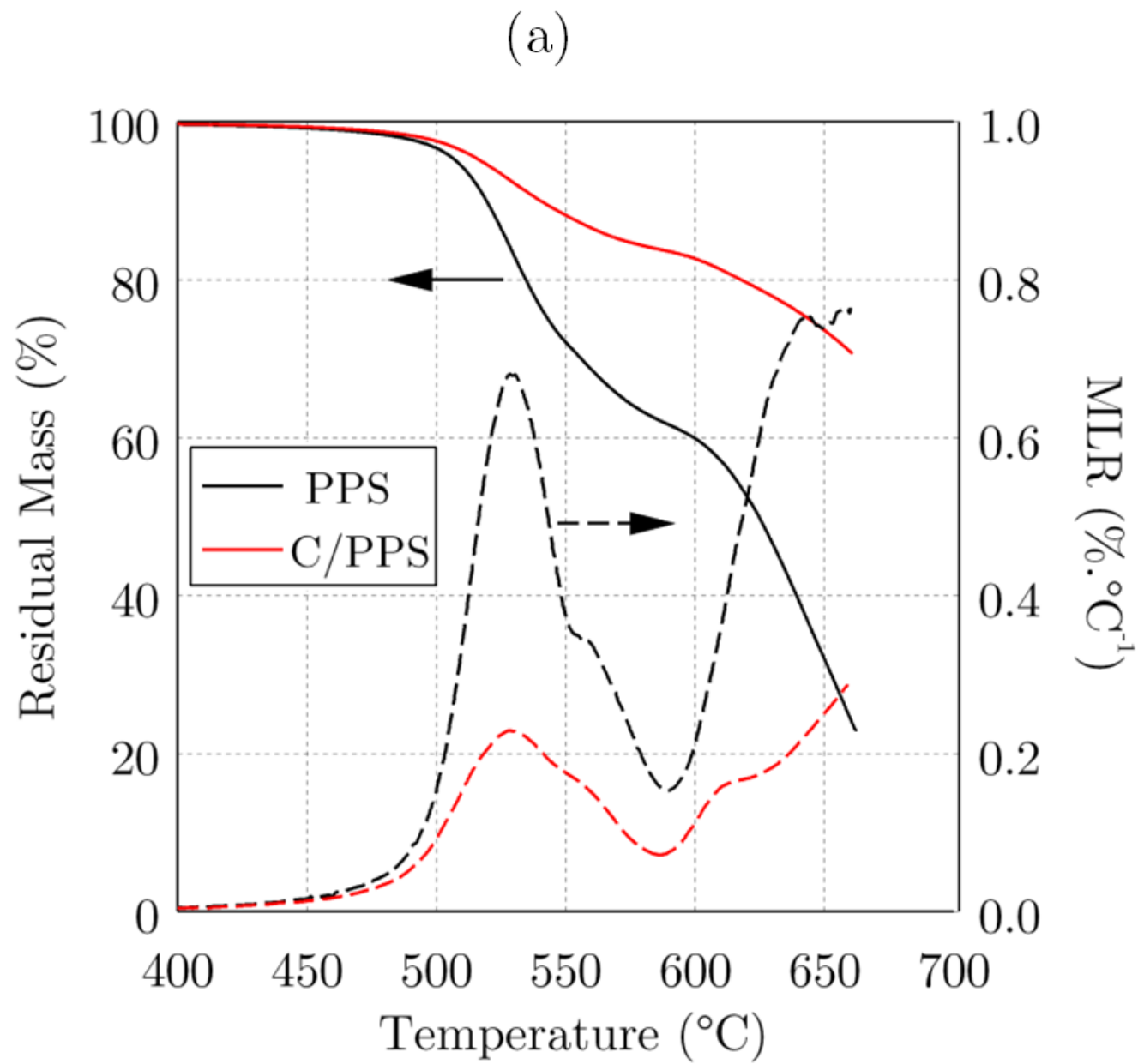




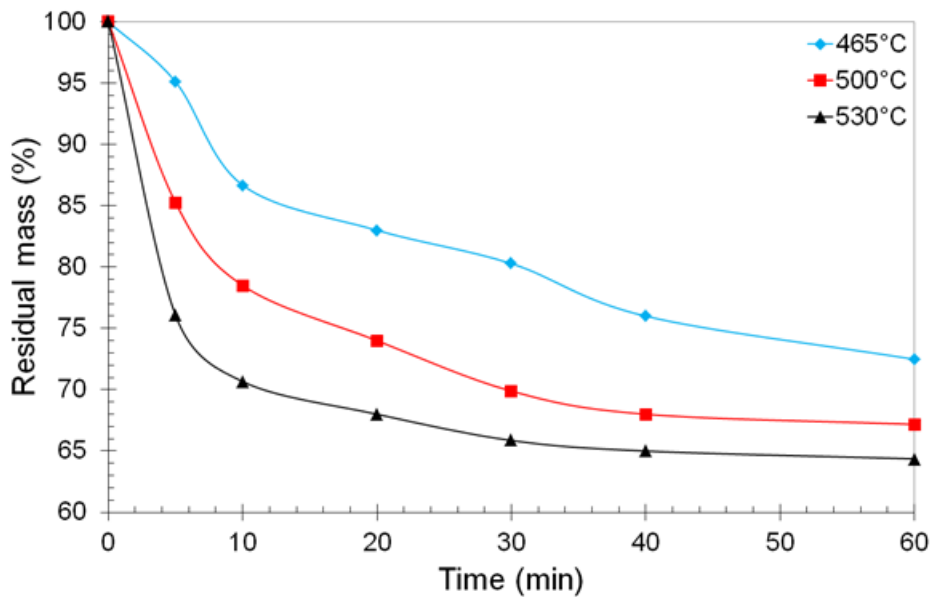




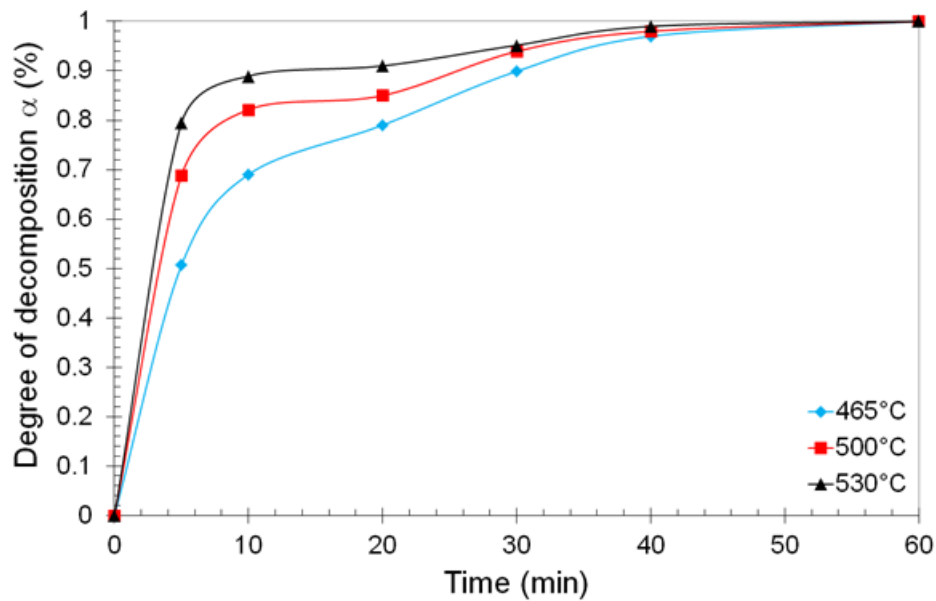


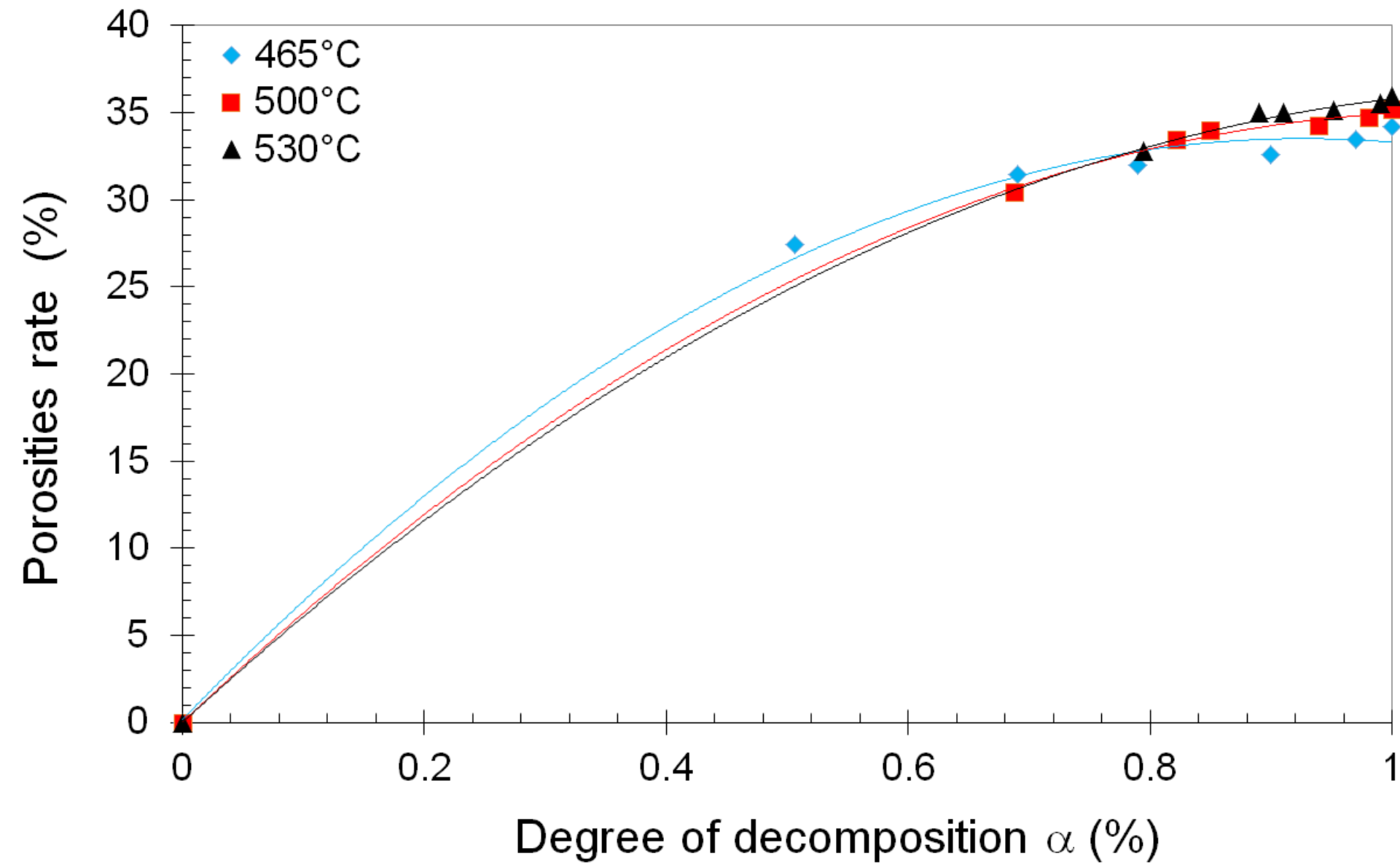


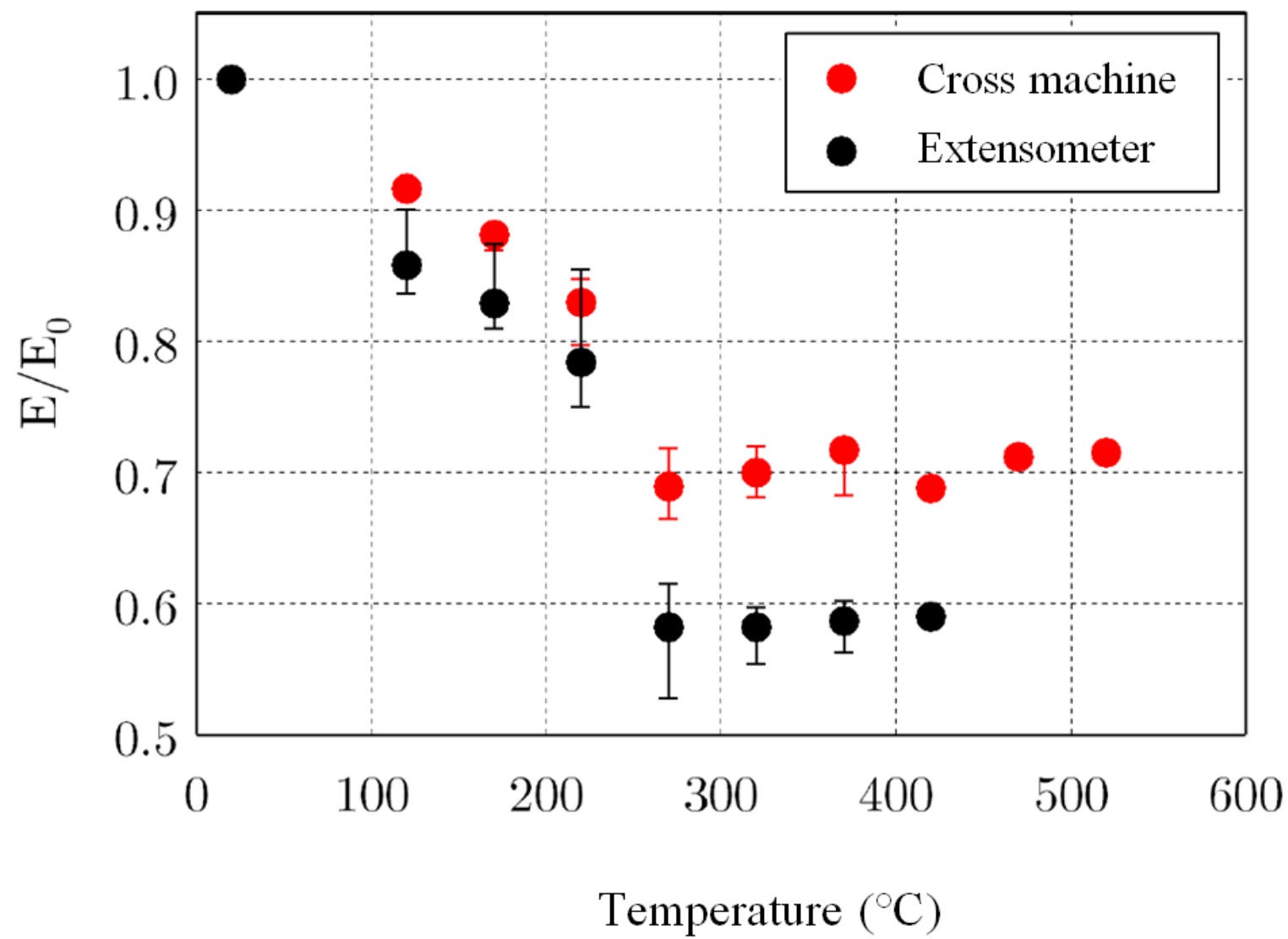
(a)



(b)



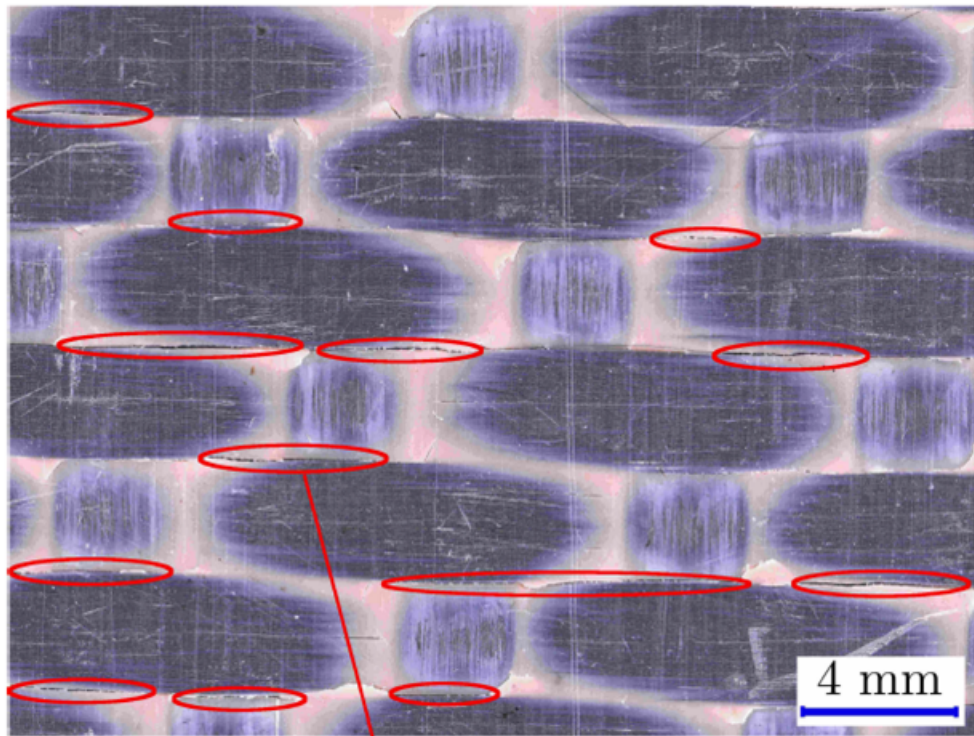




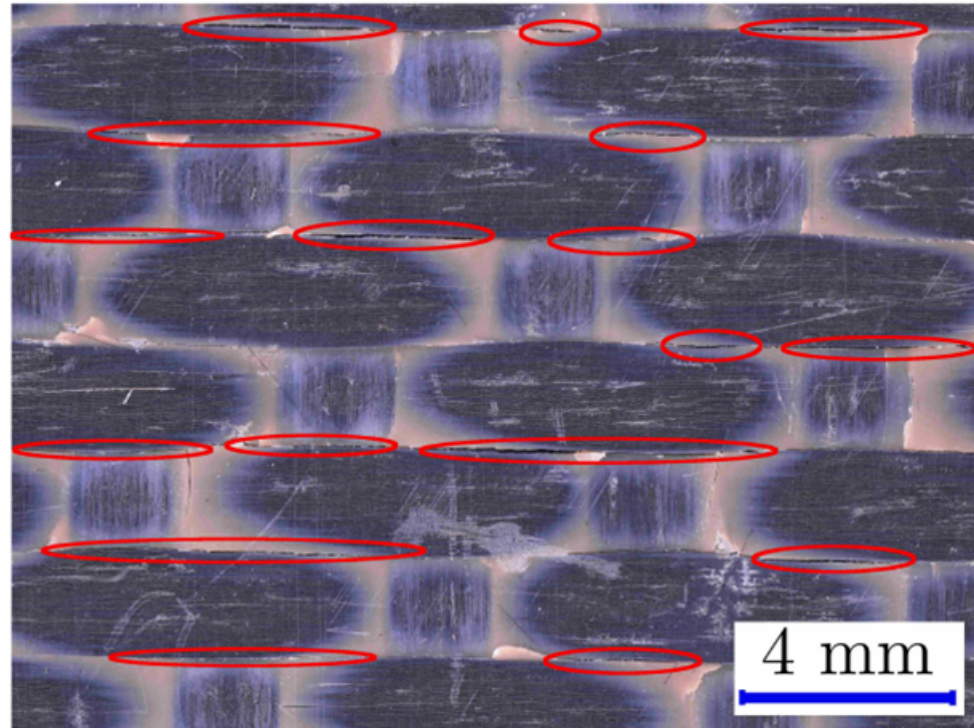
(a)

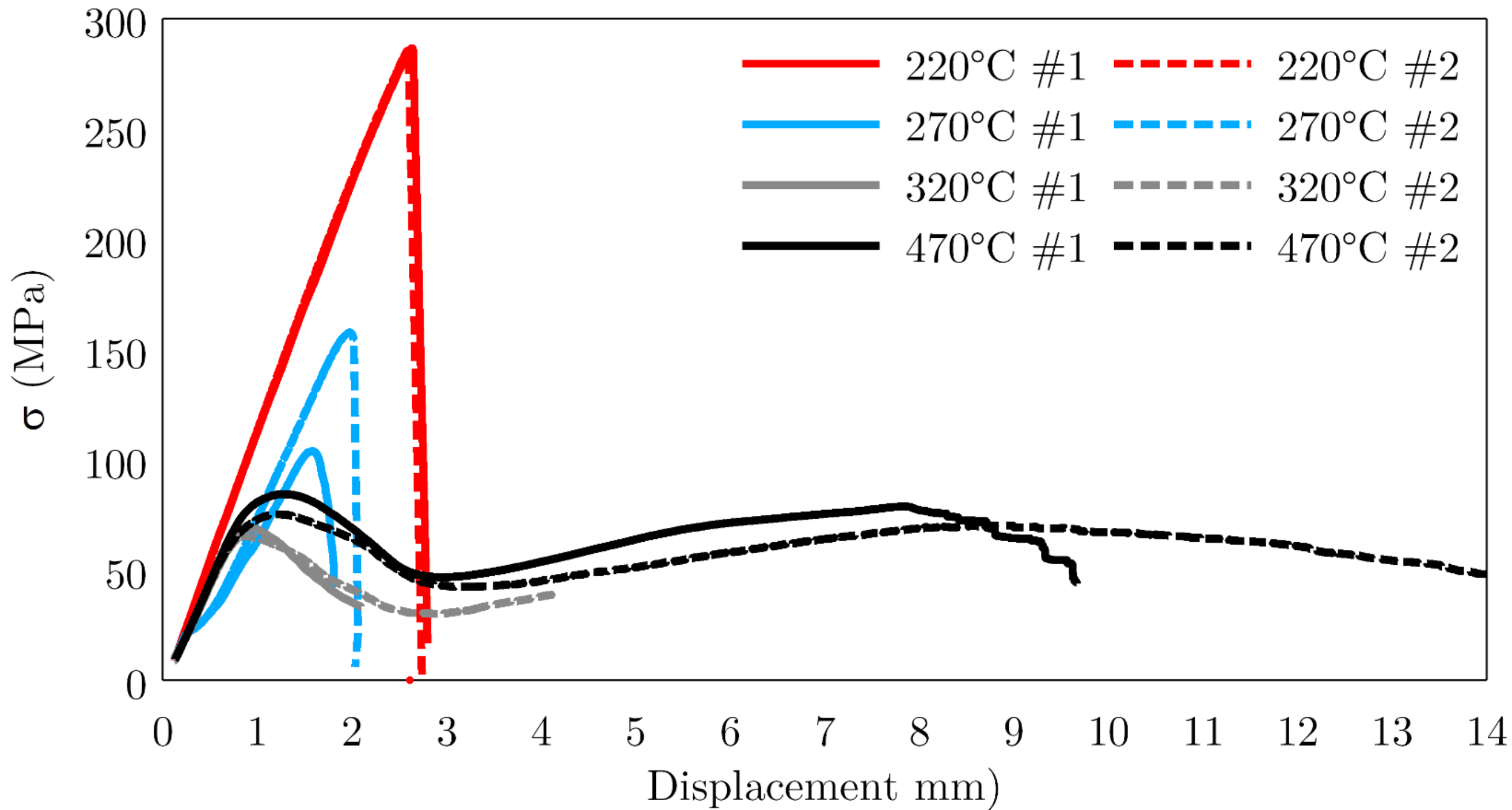
Loading direction

(b)

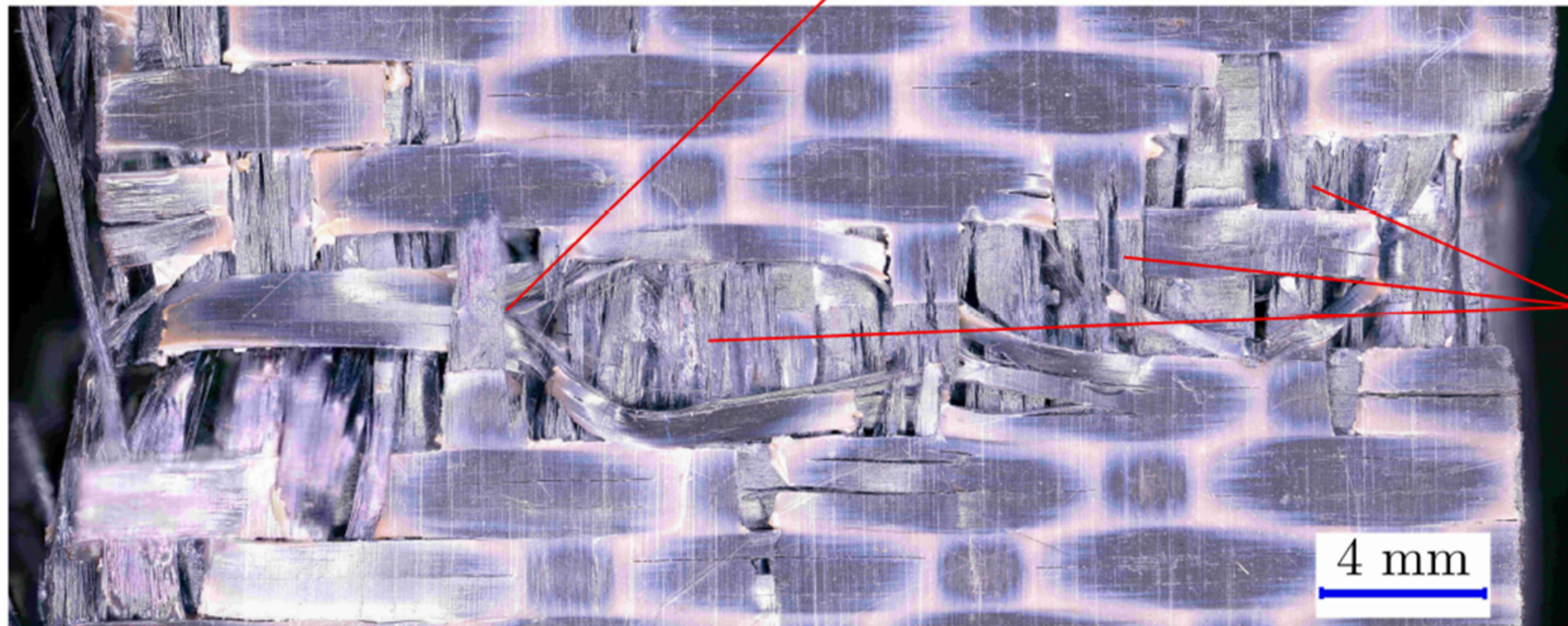


Transverse matrix cracking





Splitting of transverse strands



Transverse failure  
of longitudinal  
strands

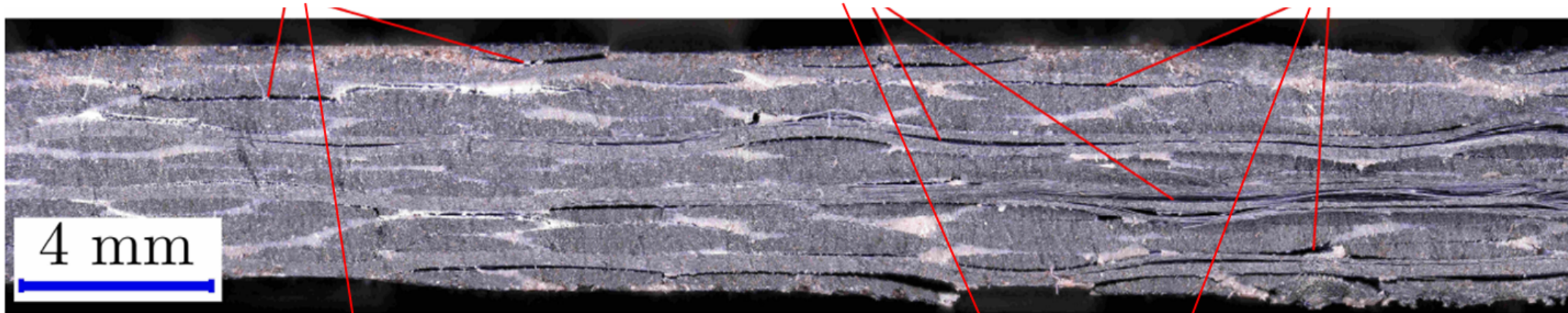
4 mm

(a)

Intra-laminar debonding

Splitting of longitudinal strands

Inter-laminar debonding

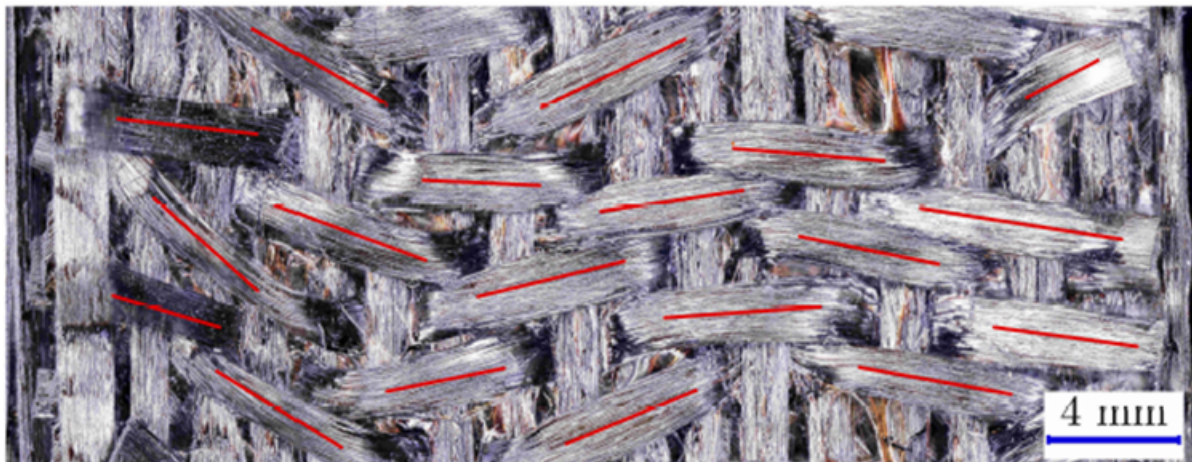


(b)





(a)



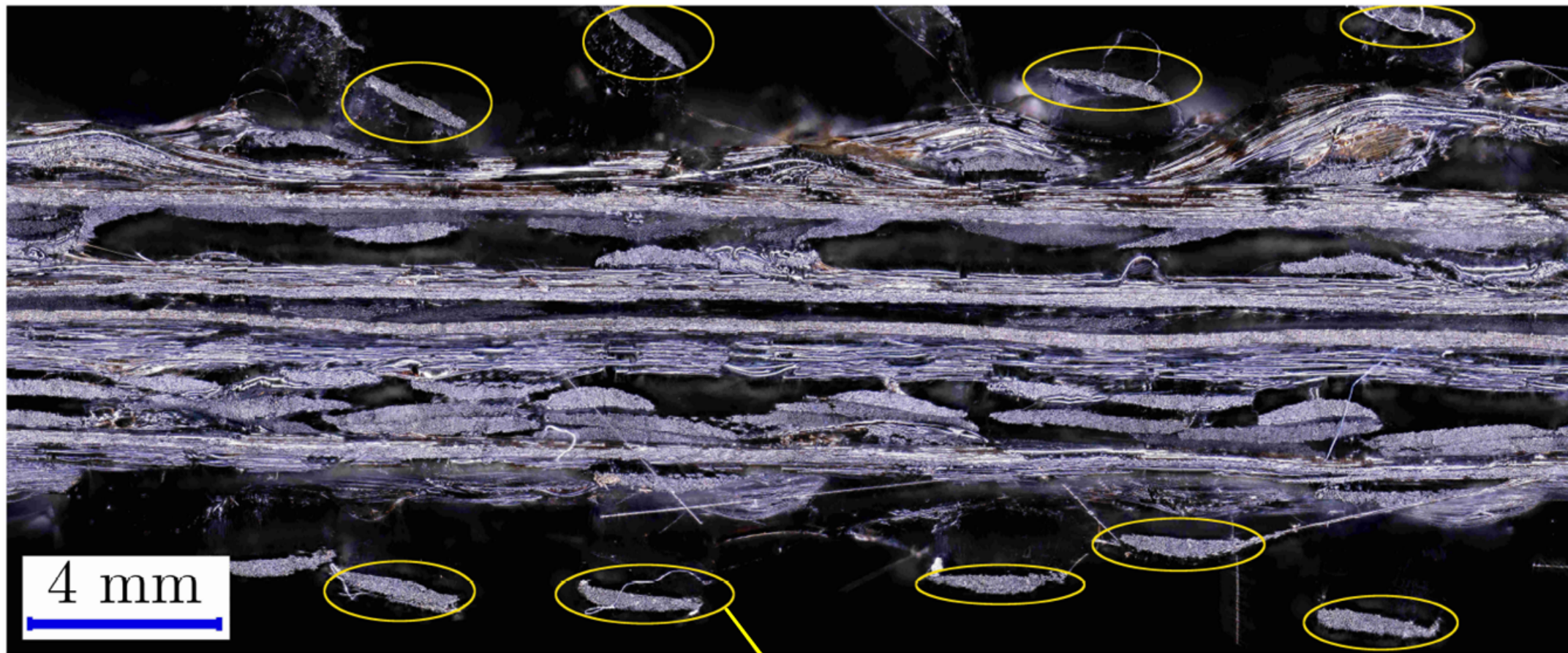
Disalignment of  
transverse strands

(b)

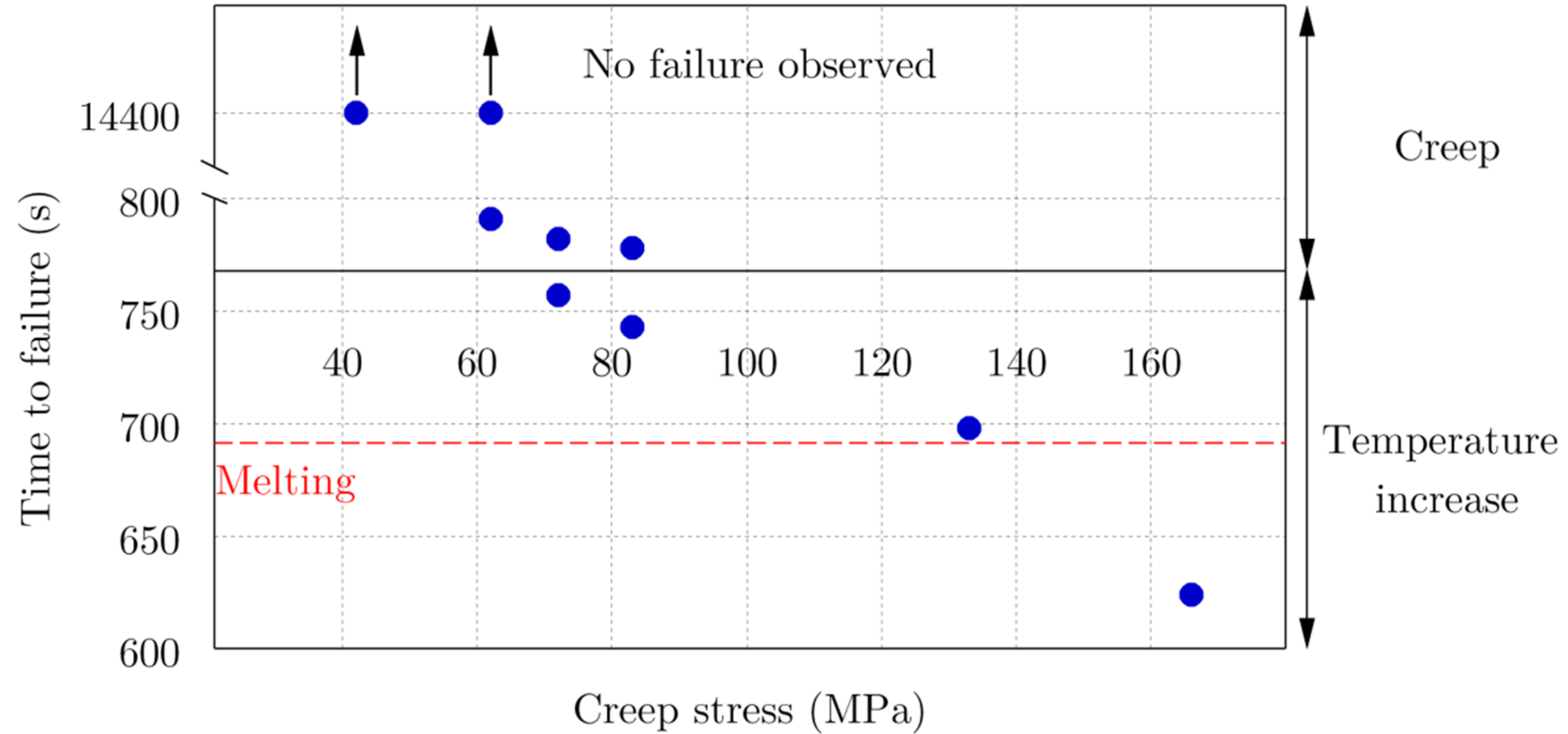


Crushing of  
transverse strands

Generalized  
necking of  $0^\circ$   
strands



Delamination and bending of the transverse strands on the external plies



## Tables

	N <sub>2</sub>	O <sub>2</sub>	Air
Plain PPS resin	503°C	502°C	508°C
C/PPS composite	483°C	515°C	517°C

Table 1 - Temperature at the onset of decomposition of plain PPS and C/PPS composites under different atmospheres

	RT	220°C	270°C	320°C	470°C
$\sigma_u$ (MPa)	514±8	286±1	131±38	68±3	80±6

Table 2 – Evolution of the ultimate tensile strength with temperature